Supporting Information

Facile and Scalable Engineering of Heterogeneous Microstructure for Uniform, Stable and Fast Lithium Plating/Stripping

Xianshu Wang,[a] Jingchun Zhuang,[a] Mingzhu Liu,[a] Cun Wang,[a] Yaotang Zhong,[a] Huirong Wang,[a] Xueqiong Cheng,[a] Si Liu,[a] Guozhong Cao,[b,*] Weishan Li,[a,c,*]

[a] School of Chemistry and Environment, South China Normal University, Guangzhou 510006, China

[b] Department of Materials Science and Engineering, University of Washington, Seattle, Washington 98195, United States

[c] National and Local Joint Engineering Research Center of MPTES in High Energy and Safety LIBs, Engineering Research Center of MTEES (Ministry of Education), and Key Lab. of ETESPG(GHEI), South China Normal University, Guangzhou 510006, China

*Corresponding authors: gzcao@u.washington.edu; liwsh@scnu.edu.cn.

1. Experimental Section

Electrode preparation: The heterogeneous microstructure was engineered on Li metal via a solid-state conversion reaction of zinc phosphate (ZPO) with Li (Figure 1a). The Li foils were purchased from Tianjin China Energy Lithium Co. Ltd with a purity of 99.9%. ZPO was obtained by calcining $Zn_3(PO_4)_2$ $4H_2O$ (98+%, Adamas) with argon atmosphere at 350 ^oC for 2 h Typically, the white and insoluble ZPO powder reserved in a bottle (**Figure S1**) was dispersed onto fresh Li scraped metal surface. Then, the Li metal was rolled repeatedly until the color of Li metal surface was changed. The resulting Li foil was cut into a disk with a diameter of 12 mm as working electrode (ZPO-Li) for coin cell test, or a large electrode (length 60 mm × width 48 mm) for pouch cell test. These processes were performed in an argon-filled glove box with moisture and oxygen contents less than 0.1 ppm. To obtain the loading of composite texture, the modified Li anode was dissolved in ethanol and then collected by vacuum filtration for weighing. The loading of composite texture are about 1.4 mg cm^{-2}. The small-size $Zn_3(PO_4)_2$ nano-powder was obtained by high-speed ball milling at a speed of 235 rpm min^{-1} with the calcined $Zn_3(PO_4)_2$ powder precursor, labeled as "N-ZPO".

Materials characterizations: The surface morphology was characterized on a field-emission scanning electron microscope (FESEM, FEI 250G) operated at a high voltage of 20 kV. The heterogeneous microstructure was confirmed through a transmission electron microscope (TEM, FEI Talos F200). The TEM sample was collected from the surface scraping of ZPO-Li, which was dispersed in carbonate as solvent under ultrasonicating, dropped onto the carbon supported membrane, and dried in the Ar-filled glove box. Powder X-ray diffraction (XRD, Rigaku Ultima V) was operated with Cu Kα radiation (λ = 0.15406 nm) and 2θ in the range of 10° to 90° at 1° min^{-1} to examine the components of the microstrucutre. The surface chemistry was qualitatively analyzed by X-ray photoelectron spectra

(XPS, ESCALAB 250). The cycled electrodes were rinsed with carbonate and dried in a vacuum chamber overnight before analysis. The XPS and SEM samples were prepared in the Ar-filled glove box and transferred to testing chamber using transfer vessel.

Electrochemical tests: The undecorated carbonate-based electrolyte was 1 M lithium hexafiluorophosphate ($LiPF_6$) dissolved in a 1:1:1 (by weight) mixture of ethylene carbonate (EC), ethyl methyl carbonate (EMC), dimethyl carbonate (DEC) with no additive. For the optimization of electrolyte for further reinforcing cycling stability, 10 wt. % fluoroethylene carbonate (FEC) was employed as electrolyte additive. The liquid electrolytes used in each coin cell were 70 μL, which is enough to free from drying up of electrolyte. The symmetric cells were assembled with the ZPO-Li or freshly scraped Li (as a control, denoted as "bare Li") electrodes (diameter = 12 mm, thickness = 450 μm) into 2025-type coin cell at room temperature, with Celgard 2400 as separator. The electrochemical cycling was conducted on a Land testing system with galvanostatic conditions. The areal Li plating/stripping capacity was set to 1 or 3 mA h cm^{-2} at various current densities from 1 to 5 mA cm^{-2}. As to the preparation of lithium iron phosphate ($LiFePO_4$) electrode, 80 wt. % $LiFePO_4$ powder, 10 wt. % acetylene black, and 10 wt. % polyvinylidene fluoride were mixed in the N,N-dimethyl-2-pyrrolidinone to form a slurry, and then casted on to the Al foil. The whole piece of $LiFePO_4$ electrode was fully dried in the vacuum oven (120 ^oC), followed by punching into a circular electrode with a diameter of 12 mm and a large square electrode (length 57 mm × width 44 mm) (**Figure S19**) and a mass loading of about 6.37-6.50 mg cm^{-2}, for coin cell and pouch cell, respectively. The assembly of coin and pouch cell was executed with $LiFePO_4$ as cathode, bare Li or ZPO-Li as anode, and Celgard 2400 as separator in a traditional method. The Celgard 2400 separator was sandwiched between $LiFePO_4$ cathode and Li anode, and then sealed by stainless steel coin shell or an Al-plastic film. The Li‖$LiFePO_4$ cells were cycled in

the potential range of 2.2 ~ 4.1 V (*vs.* Li/Li^+) at different rates from 0.2 to 4 C (1 C = 170 mA g^{-1}). The galvanostatic and rate charge/discharge curves were recorded by a Land tester at different current densities. The specific capacity and areal capacity are calculated based on the mass of $LiFePO_4$. The $Li_4O_5Ti_{12}$ electrode was prepared by the similar method as $LiFePO_4$ electrode, and its areal capacity was controlled to 7.3 mg cm^{-2}, about 1.34 mA h cm^{-2}. The Li||$Li_4Ti_5O_{12}$ cells were cycled in the voltage range from 1.0 to 2.5 V (*vs.* Li/Li^+) at various rates of 0.2, 0.5, 1, 2, 3 and 5 C (1 C = 175 mA g^{-1}). The electrochemical impedance spectroscopy (EIS) of symmetric cells and asymmetric cells were carried out on an electrochemical work station (Metrohm Autolab/PGSTAT30) from 200 kHz to 0.01 Hz and 100 kHz to 0.01 Hz with a voltage amplitude of 10 mV, respectively.

Theoretical calculations: The calculations using *Gaussian 09* package[1] were performed to optimize the compounds with B3LYP in conjunction with the 6-311++G(d) level basis for confirming their energy levels and Gibbs free energy. Polarized continuum models (PCM) were used to investigate the bulk solvent effect (dielectric constant is 20.5). The frequency calculations were performed at the same level to confirm that every optimized structure corresponded to a stationary one. Besides, the calculations about binding energy were conducted in the Vienna *ab* initio simulation package (VASP)[2, 3] with general gradient approximation (GGA) of Perdew-Burke-Ernzerhof (PBE)[4] exchange-correlation function. The energy cutoff was set to 500 eV. The self-consistent field (SCF) and geometry convergence tolerance were set to 1×10^{-5} eV and 1×10^{-4}, respectively. For Li (110), LiZn (111) and LiZn (220) crystal face model, a five-layer 2×2×1 super cell with a 1.5 nm vacuum was adopted. When calculating the Li binding energy, only the bottom two-layer atoms were fixed and the others were fully relaxed. The k-points for Brillioun zone were selected by Monkhorts-Pack method[5] and set to 4×4×1 for Li and LiZn slab. The binding energy,

E_b, was defined as

$$E_b = E_{total} - E_{slab} - E_{Li}$$

where E_{total}, E_{slab}, and E_{Li} are the total energy of LiZn/Li slab bound with Li atom, the pristine LiZn/Li slab, and single Li atom, respectively.

2. Supporting Figures

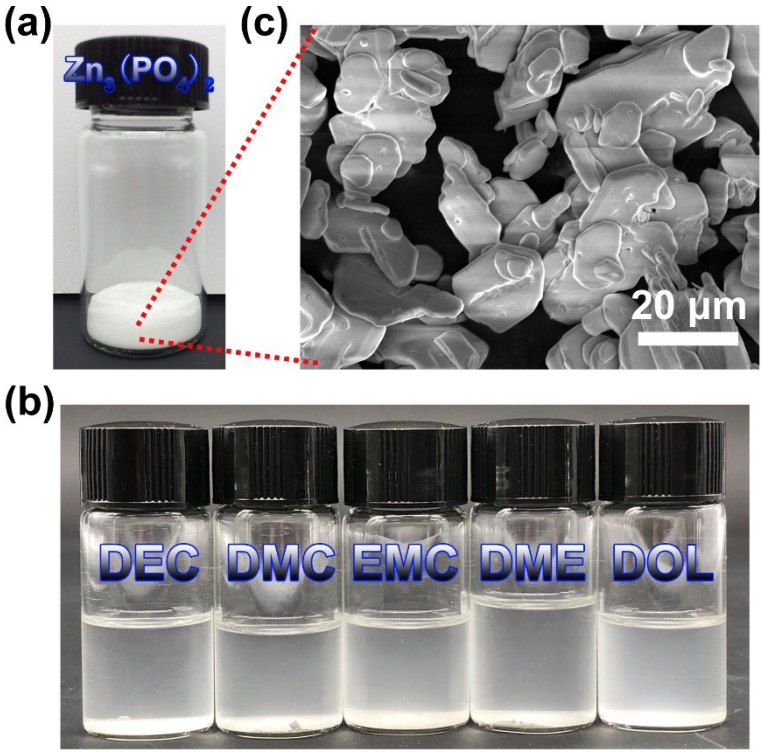

Figure S1. Digital photos of (a) $Zn_3(PO_4)_2$ powder and (b) 0.2 wt.% $Zn_3(PO_4)_2$ suspended in carbonate or ether solvent. (c) SEM image of $Zn_3(PO_4)_2$ powder. These are indicative of the white color, the insolubility in carbonate or ether solvent and the particle appearance of $Zn_3(PO_4)_2$.

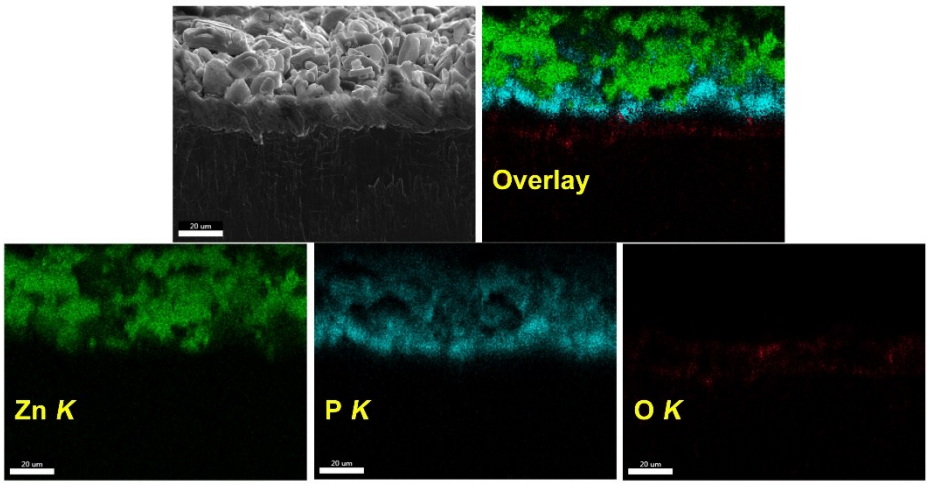

Figure S2. The SEM image of the engineered heterogeneous microstructure under cross-sectional view and corresponding elemental mappings.

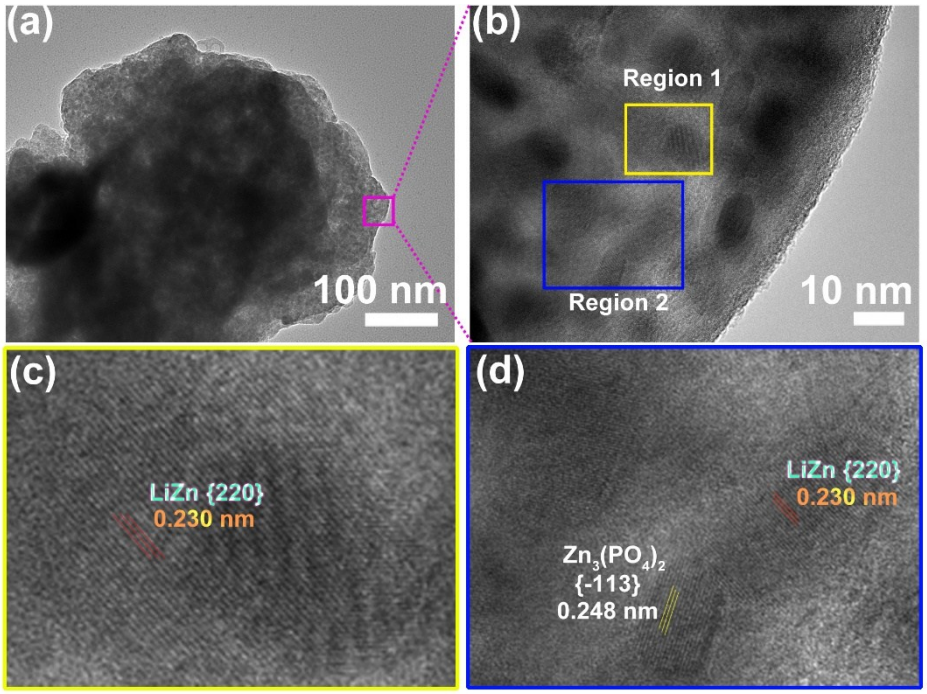

Figure S3. (a) Low-magnification and (b) high-resolution TEM images of the particles in the the engineered heterogeneous microstructure. (c, d) Magnified TEM images are corresponding to the yellow region 1 and blue region 2 outlined in (b), respectively.

As shown in Fig. S3d, residual ZPO particles is still identified, which is attributed to the incomplete conversion reaction under rolling. These particles can serve as a scaffold for anchoring the as-formed heterogeneous microstructure, increasing the cyclic stability of ZPO-Li electrode.

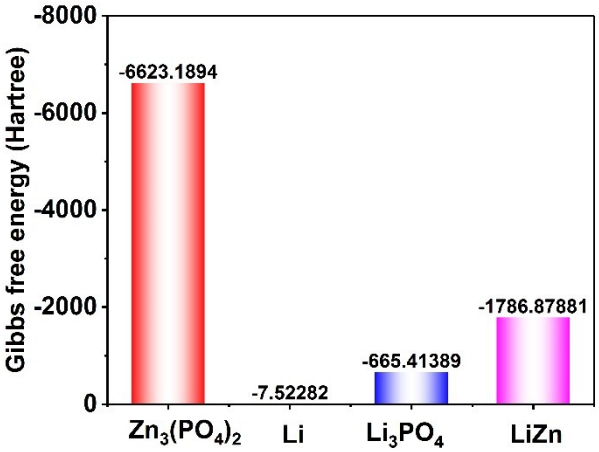

$Zn_3(PO_4)_2 + 9Li = 2Li_3PO_4 + 3LiZn$

ΔG = -0.5694 Hartree = -1494.96 KJ mol^{-1}

Figure S4. The Gibbs free energy change (ΔG) for the reaction of $Zn_3(PO_4)_2$ with Li metal, indicative of the spontaneity of ion-exchange.

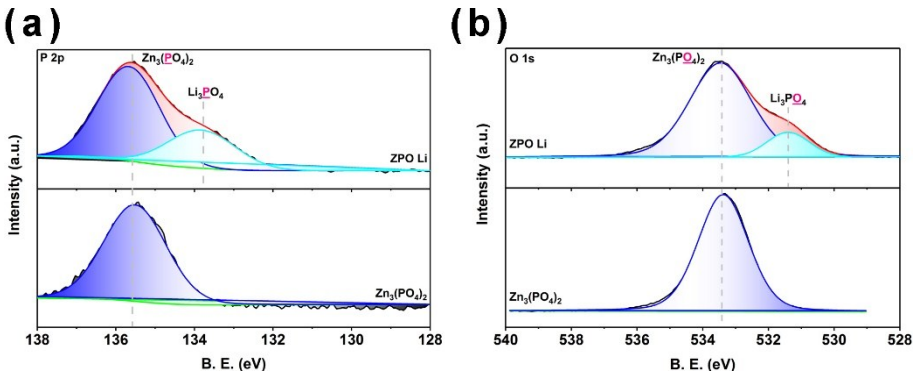

Figure S5. XPS spectra of (a) Zn 3s and P 2p and (b) O 1s of pure $Zn_3(PO_4)_2$ powder and ZPO-Li.

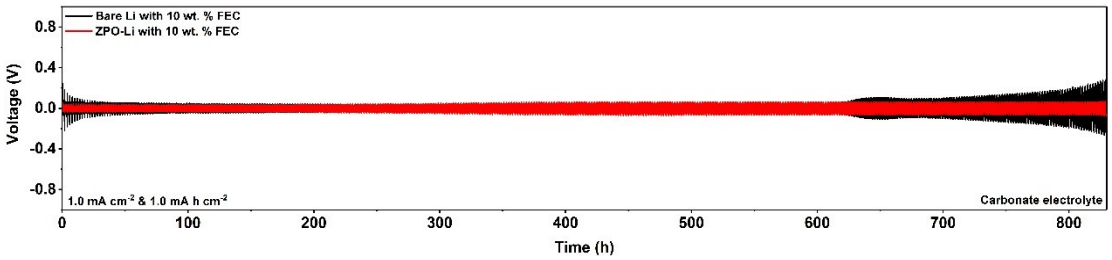

Figure S6. The voltage profiles of bare Li- and ZPO-Li-based symmetric cells with Li plating/stripping capacity of 1.0 mA h cm^{-2} at a current density of 1.0 mA cm^{-2} in the presence of 10 wt. % fluoroethylene carbontate (FEC).

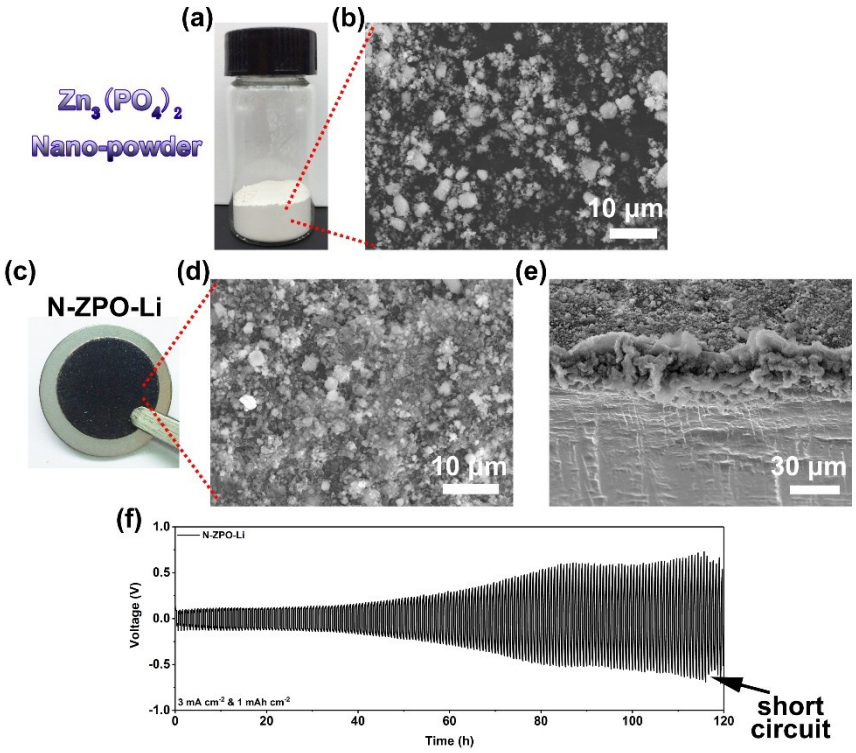

Figure S7. (a) Digital photo and (b) SEM image of $Zn_3(PO_4)_2$ nano-powder. (c) Digital photo and (d) top-view and (e) cross-sectional SEM image of surface-treated Li foil using $Zn_3(PO_4)_2$ nano-powder (N-ZPO-Li). (f) The Li plating/stripping profiles of N-ZPO-Li anode in symmetric cell at 3.0 mA cm^{-2} with a Li capacity of 1.0 mA h cm^{-2}.

To understand the effect of $Zn_3(PO_4)_2$ particle size, ultrafine white $Zn_3(PO_4)_2$ nanopowder (N-ZPO, Fig. S7a, b) was transferred on the Li surface. After rolling, the Li surface is turned to be dark black (Fig. S7c-e), indicating the more complete reaction of $Zn_3(PO_4)_2$ with Li metal. When applied in the symmetric cell, N-ZPO-Li anode offers the cycling less than 120 h at 3.0 mA cm^{-2} with Li capacity of 1.0 mA h cm^{-2}(Fig. S7f), which is far poorer than that of ZPO-Li electrode (Fig. 3b). This difference suggests that the $Zn_3(PO_4)_2$ particle size affects the electrochemical performance of the Li electrode. More compact surface resulting from the smaller $Zn_3(PO_4)_2$ particles cannot accommodate larger Li capacity, leading to more electrolyte decomposition and dendrite growth.

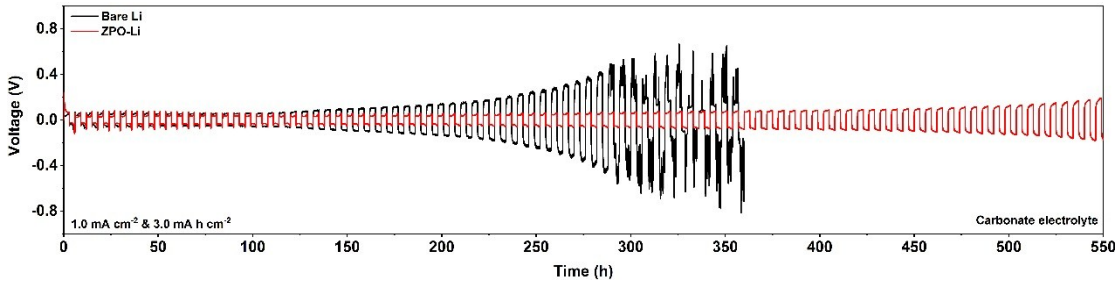

Figure S8. The Li plating/stripping profiles of bare Li and ZPO-Li electrodes in symmetric cell at a current density of 1.0 mA cm^{-2} with a Li capacity of 3.0 mA h cm^{-2}.

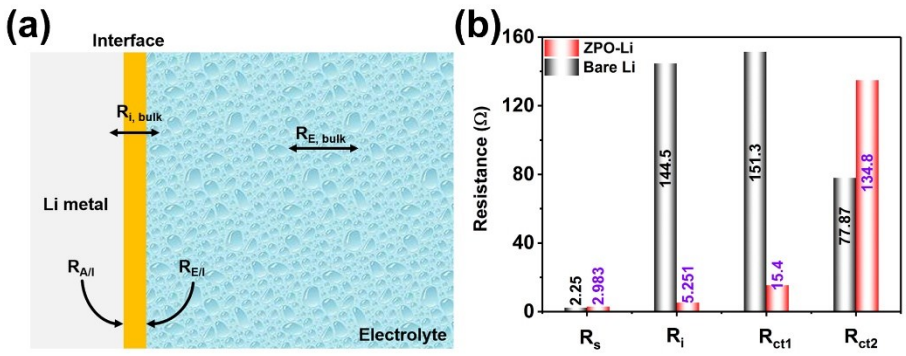

Figure S9. (a) Schematics of resistance contributions in Li‖Li symmetric cells after cycling ($R_{E, bulk}$: the bulk resistance of liquid electrolyte; $R_{i, bulk}$: the bulk resistance of interface layer; $R_{charge\ transfer}$: the charge transfer resistance, including $R_{A/I}$ and $R_{E/I}$. The former relates to the resistance between anode and interface, and the latter involves the resistance between electrolyte and interface). (b) The fitting results of electrochemical impedance spectra for bare Li- and ZPO-Li-based symmetric cell after 3 cycle formation.

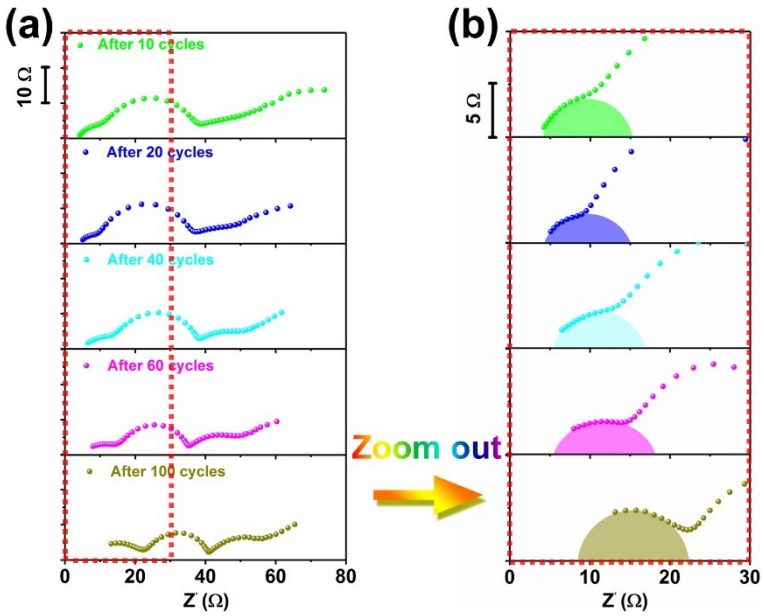

Figure S10. Ex-situ EIS test of ZPO-Li electrodes in Li‖Li symmetric cells after different cycles under a current density of 1.0 mA cm^{-2}. The first semicircle that reflects on the bulk resistance of interface layer can basically maintain unchanged after fitting, indicative of the good interfacial stability.

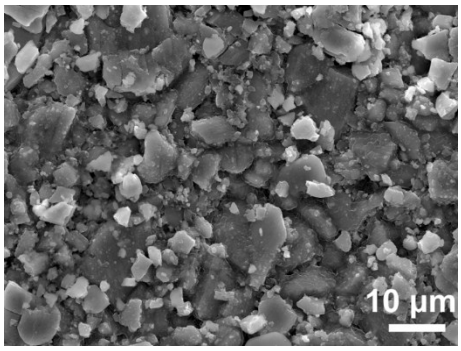

Figure S11. SEM image of low-capacity Li plating (0.2 mA h cm^{-2}) on the ZPO-Li electrode at 0.5 mA cm^{-2}, presenting that the Li is uniformly deposited in the as-engineered heterogeneous microstructure.

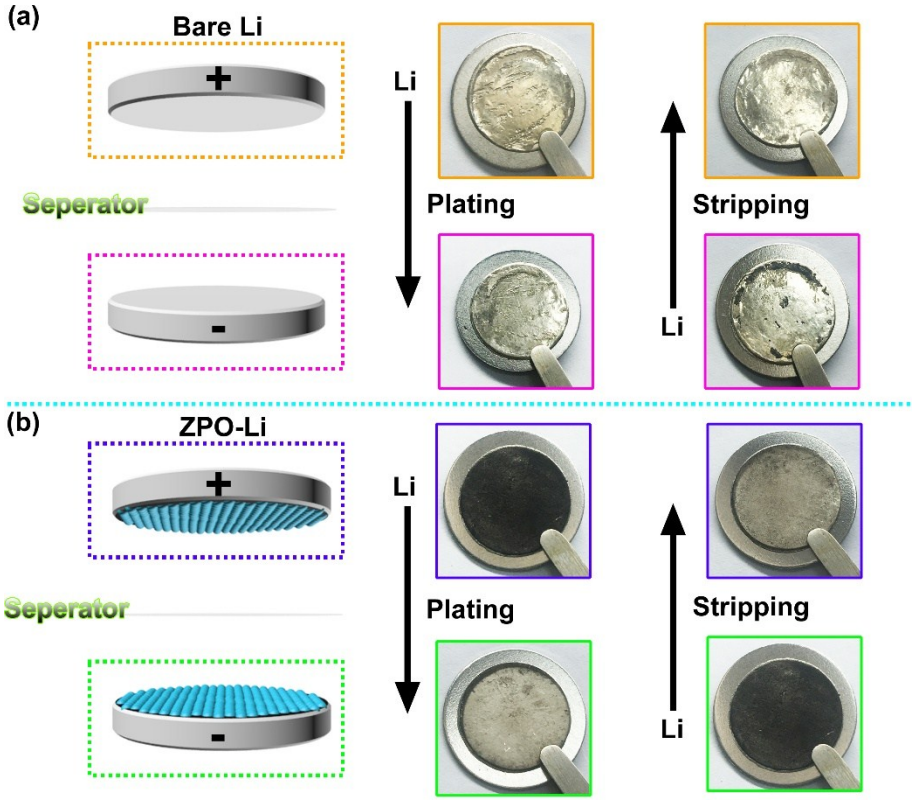

Figure S12. The schematics and digital photos of (a) bare Li and (b) ZPO-Li electrodes after 1st plating and stripping. The different surface morphology at macro level further confirms ZPO powder treatment yields a uniform Li plating/stripping instead of local-distributed Li deposition/dissolution in the cell with bare Li.

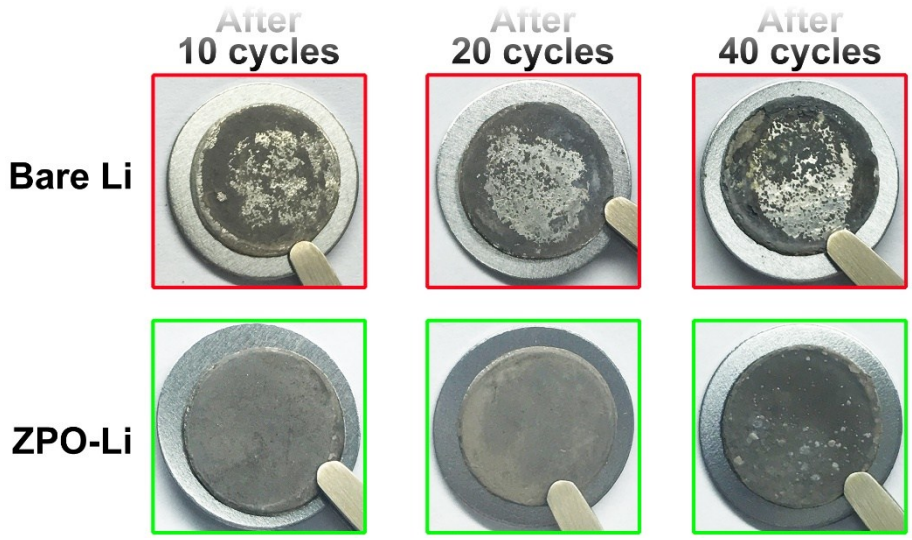

Figure S13. The digital photographs of bare Li (red box) and ZPO-Li (green box) electrodes after 10, 20 and 40 cycles.

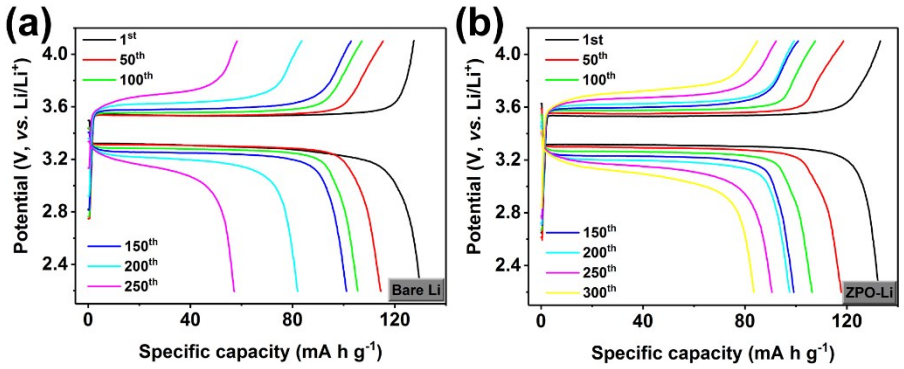

Figure S14. The voltage-capacity profiles of (a) bare Li‖$LiFePO_4$ and (b) ZPO-Li‖$LiFePO_4$ batteries at a rate of 1 C (1 C = 170 mA g^{-1}) for the selected cycles.

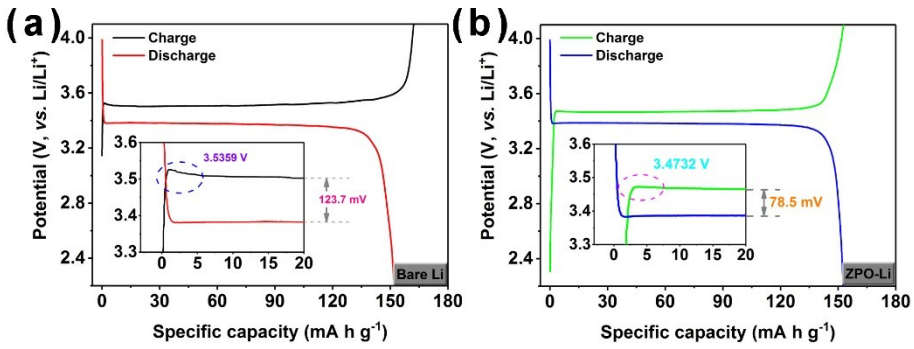

Figure S15. The voltage hysteresis of (a) bare Li‖$LiFePO_4$ and (b) ZPO-Li‖$LiFePO_4$ batteries based on the charge/discharge profiles of the initial cycle at 0.2 C (1 C = 170 mA g^{-1}).

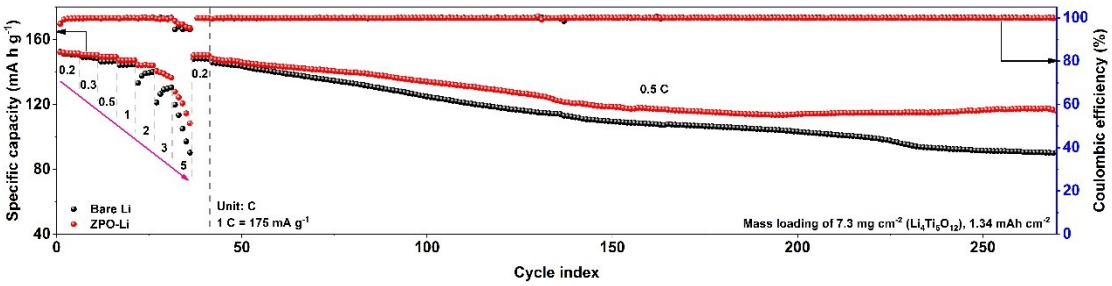

Figure S16. The rate capability at different rates from 0.2 to 5 C (1 C = 175 mA g^{-1}) and long-term cyclic stability at a rate of 0.5 C of bare Li‖$Li_4Ti_5O_{12}$ and ZPO-Li‖$Li_4Ti_5O_{12}$ batteries.

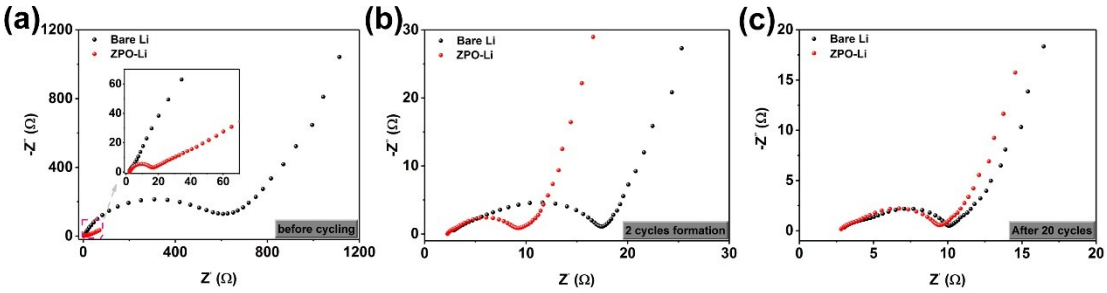

Figure S17. Nyquist plots of bare Li‖$Li_4Ti_5O_{12}$ and ZPO-Li‖$Li_4Ti_5O_{12}$ batteries (a) before cycling, after (b) 2 cycles formation and (c) 20 cycles.

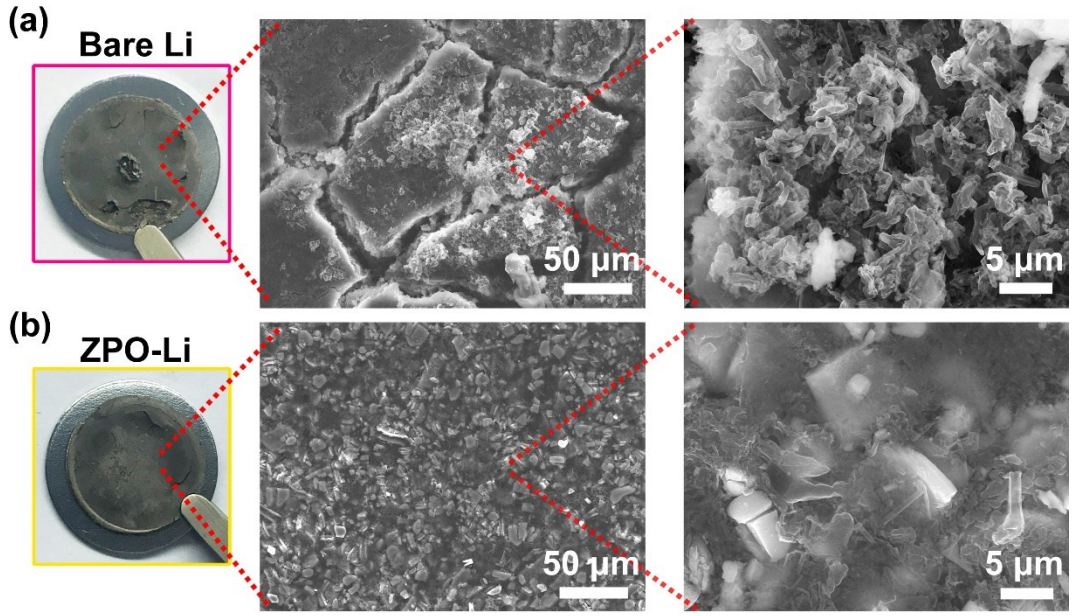

Figure S18. The digital photographs and SEM images of (a) bare Li and (b) ZPO-Li anode after cycling in the $Li_4Ti_5O_{12}$-based batteries.

The bare Li anode in $Li_4Ti_5O_{12}$-based battery presents worse surface damage (Fig. S18a) than that in $LiFePO_4$-based battery (Fig. 5f), which is related to the initial lithium striping that is necessary for $Li_4Ti_5O_{12}$-based battery. In contrast, ZPO-Li anode in $Li_4Ti_5O_{12}$-based battery reserves its surface integrity (Fig. S18b) as it behaves in $LiFePO_4$-based battery (Fig. 5g), except for the observable heterogeneous microstructure due to the less electrolyte decomposition in $Li_4Ti_5O_{12}$-based battery.

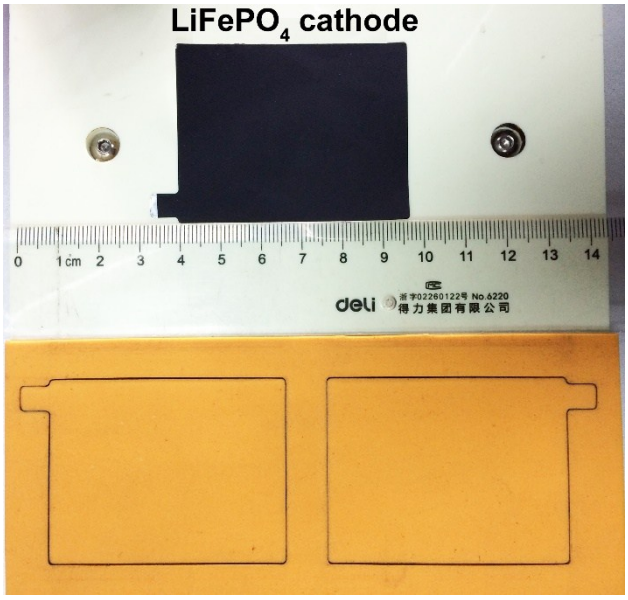

Figure S19. The optical image of scale-up $LiFePO_4$ cathode cut by die-cutter.

References

[1] M. J. Frisch, G. W. Trucks, H. B. Schlegel, G. E. Scuseria, M. A. Robb, J. R. Cheeseman, G. Scalmani, V. Barone, B. Mennucci, G. A. Petersson, H. Nakatsuji, M. Caricato, X. Li, H. P. Hratchian, A. F. Izmaylo, J. Bloino, G. Zheng, J. L. Sonnenberg, M. Hada, M. Ehara, K. Toyota, R. Fukuda, J. Hasegawa, M. Ishida, T. Nakajima, Y. Honda, O. Kitao, H. Nakai, T. Vreven, J. A. Jr. Montgomery, J. E. Peralta, F. Ogliaro, M. Bearpark, J. J. Heyd, E. Brothers, K. N. Kudin, V. N. Staroverov, R. Kobayashi, J. Normand, K. Raghavachari, A. Rendell, J. C. Burant, S. S. Iyengar, J. Tomasi, M. Cossi, N. Rega, J. M. Millam, M. Klene, J. E. Knox, J. B. Cross, V. C. Bakken, Adamo, J. Jaramillo, R. Gomperts, R. E. Stratmann, O. Yazyev, A. J. Austin, R. Cammi, C. Pomelli, J. W. Ochterski, R. L. Martin, K. Morokuma, V. G. Zakrzewski, G. A. Voth, P. Salvador, J. J. Dannenberg, S. Dapprich, A. D. Daniels, Ö. Farkas, J. B. Foresman, J. V. Ortiz, J. Cioslowski, and D. J. Fox, *Gaussian 09*, Revision A, Gaussian, Inc, Wallingford, CT, 2009.

[2] G. Kresse, and J. Furthmüller, *Comput. Mater., Sci.,* 1996, **6**, 15;

[3] G. Kresse, and J. Furthmüller, *Phys. Rev., B*, 1996, **54**, 11169.

[4] J. P. Perdew, and K. Burke, *Phys. Rev. Lett.,* 1996, **77**, 3865.

[5] H. J. Monkhorst, and J. D Pack, *Phys. Rev. B,* 1976, **13**, 5188.